

**DESIGN AND DEVELOPMENT OF POLYMER
ALTERED LIQUID CRYSTAL FOR ELECTRO-
OPTIC AND THERMOELECTRIC
APPLICATIONS**

ASHA KUMARI



**DEPARTMENT OF PHYSICS
INDIAN INSTITUTE OF TECHNOLOGY DELHI
JULY 2023**

© Indian Institute of Technology Delhi (IITD), New Delhi, 2023

**DESIGN AND DEVELOPMENT OF POLYMER
ALTERED LIQUID CRYSTAL FOR ELECTRO-
OPTIC AND THERMOELECTRIC
APPLICATIONS**

by

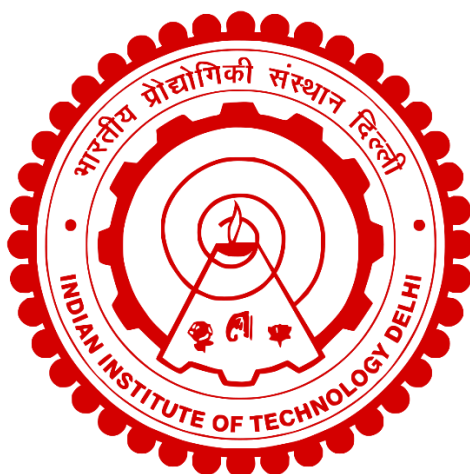
ASHA KUMARI

Department of Physics

Submitted

in fulfilment of the requirements of the degree of Doctor of Philosophy

to the



INDIAN INSTITUTE OF TECHNOLOGY DELHI

JULY 2023

Dedicated to my Parents

CERTIFICATE

This is to certify that the thesis entitled, “**Design and Development of Polymer Altered Liquid Crystal for Electro-optic and Thermoelectric Applications**”, being submitted by **Ms. Asha Kumari** to the Indian Institute of Technology Delhi for the award of the degree of **Doctor of Philosophy** is a record of bonafide research work carried out by her. She has worked under my supervision and guidance and has fulfilled the requirements for the submission of this thesis, which to the best of my knowledge has reached the requisite standard.

The contents contained in this thesis have not been submitted in part or in full to any other university or institute for the award of any degree or diploma.

Prof. Aloka Sinha

Department of Physics

Indian Institute of Technology Delhi

Hauz Khas, New Delhi-110016

ACKNOWLEDGEMENTS

I would like to take this opportunity to thank every person who has played a pivotal role in my research so far and helped me directly or indirectly to shape this thesis. First and foremost, I am deeply indebted to my supervisor Prof. Aloka Sinha who introduced me to the fascinating world of liquid crystals. Her continuous support, encouragement, and motivation have been instrumental in successfully completing this thesis. She allowed me to pursue my research interests and was always available for help or discussion. Throughout the years, she has provided me with wise counsel, sound advice, and many superior ideas, which turned out to be an exciting and rewarding learning experience. She has helped me to develop myself as a professional researcher and shaped me to become a better human being. Her optimism, kindness, and support through every thick and thin have helped me overcome all the uncertainties in my research journey so far. My appreciation for her cannot be enough; still, I would like to thank you, Madam, for being there and believing in my abilities.

I would like to thank my research committee members, Prof. Dalip Singh Mehta (Dept. of Physics, IIT Delhi), Prof. Kedar B. Khare (Dept. of Physics, IIT Delhi), and Prof. V. Haridas (Dept. of Chemistry, IIT Delhi), who devoted their precious time during research progress meetings. I am thankful to them for providing their valuable insights, suggestions, and constant encouragement regarding research work during the entire period.

I gratefully acknowledge our scientific collaborators, with whom I have had the opportunity and privilege to work. I am grateful to Prof. V. Haridas, Dr. Sameer Dhawan, Mr. Hanuman Singh, and Mr. Surya Kant Bhardwaj of the Dept. of Chemistry, IIT Delhi, for providing the pseudopeptidic polymer compounds and for the valuable and in-depth discussions on the collaborative work. Prof. Bodh Raj Mehta for providing the thermoelectric characterization setups, and Mr. Abhishek Ghosh (Dept. of Physics, IIT Delhi) for discussions on the collaborative work.

I would like to acknowledge the central research facility (CRF), the nanoscale research facility (NRF), the Physics Department, IIT Delhi, and the Chemistry Department, IIT Delhi for providing me with the research facilities. University grant commission (UGC) is gratefully acknowledged for providing Ph.D. research fellowship during this tenure. I also acknowledge IIT Delhi and UGC, India, for the financial support to attend various conferences and workshops in India and abroad. I express my sincere thanks to the faculty and the staff members of the Physics department, IIT Delhi, for their cooperative and supportive attitude and for being of great help.

I wish to express my sincere thanks and warm regards to my lab mates and colleagues, Dr. Mukesh Sharma, Dr. Pradeep Kumar, Dr. Amina Nafees, Dr. Sourav Patranabish, Dr. Susanta Chakraborty, Mr. Ashutosh Mohan, Ms. Aysha Rani, Mr. Rahul Panchal, Ms. Shilpi Bose, Mr. Vaibhav Sharma, Mr. Rishikesh Kushawaha, Mr. Deepak Verma, Mr. Dhananjoy Mandal, Mr. Harish Khan, Mr. Kaustav Jit Bora, Mr. Debashish Bagh, Mr. Ram Ashish Yadav, Ms. Akriti, Mr. Aman and Mr. Deepak Kararwal. Their unconditional help and support in both experimental and non-experimental works have helped me greatly in achieving completion of this thesis.

I am grateful to all my friends from IIT Delhi, Dr. Madan Sharma, Ms. Priya Deshwal, Ms. Hemlata Panghal, Mr. Abhishek Ghosh, Mr. Hemant Sharma, Mr. Sandeep Kumar, Ms. Neetesh Dhakar, Ms. Deepika Poonia, Mr. Arjun Yadav, Mrs. Mamta Yadav, and many others for their help, motivation, and precious company during the time away from the lab.

A section in the acknowledgement is incomplete without paying tribute to my loving parents Mrs. Rajbala Devi and Mr. Surinder Singh, and my loving brother Mr. Promod Kumar. Your unconditional support, care and sacrifice have helped me reach where I am today. Despite all the difficult circumstances and responsibilities, you have always fostered my needs, fueled my motivation, and never lost faith in me. This thesis belongs as much to them as it is to me.

Asha Kumari

ABSTRACT

Liquid crystals (LCs) can be exploited in various technological applications, including the display industry, telecommunications, biology, and optical technology. These modern uses demand distinctive LC materials with exotic properties. New liquid crystalline materials with superior properties are needed to meet the needs of the existing industry. Due to the difficulty of synthesizing novel liquid crystalline materials with improved features, composites of LC and polymer (LCPCs) have been suggested as an alternate method to enhance the various properties of LCs, with the added benefit of better mechanical strength and flexibility. LCPCs have diverse applications, such as privacy windows, optical and electro-optical devices, optical filters, switchable THz devices, energy harvesting devices, and chemical and biosensors.

Polymers can alter LCs properties by making a continuous polymer matrix with droplets of LCs in it or by creating a bicontinuous system of a polymer network that is spread out in an LCs host phase. These soft matter systems include polymer dispersed liquid crystals (PDLCs), polymer-filled liquid crystals (PFLCs), polymer self-assembly filled liquid crystals (PSALCs), and polymer-stabilized liquid crystals (PSLCs). We have investigated various physical properties of LCPCs to better understand the interactions among polymerization conditions, polymer morphology, and electro-optic behavior and utilized these systems and materials to fabricate LCs-based electro-optic and optical devices. Towards the end of the thesis, thermoelectric energy harvesting application has been explored by using a composite of nematic LC material in combination with carbon nanotubes (CNTs) and polyvinylidene fluoride (PVDF) polymer matrix, and the potential application of LCs-based thermoelectric generator for wearable electronics and flexible devices is demonstrated.

The first two chapters of the thesis cover the fundamental concepts and properties of LCs, polymers, and thermoelectricity, as well as the experimental methods and techniques used in the research. Chapter 3 presents the effect of barium titanate (BaTiO_3) nanoparticles on the performance of epoxy-resin-based PDLC devices. The study shows that adding BaTiO_3 nanoparticles enhances the device performance by decreasing the threshold voltage, saturation voltage, and rise time while increasing the contrast ratio and UV-visible absorption spectrum. Chapter 4 describes the use of bottlebrush polymers in biomedical engineering and electro-optic applications. By varying the concentrations of polymer, LC, and solvent in the composite, an array of submicron to micron-sized structures, including porous networks, particles, spheres, aggregates, and vesicles, are formed from the LC-bottlebrush polymer composite.

Additionally, the research demonstrates the construction of light-scattering switches from polymer microsphere-filled liquid crystals (PFLCs) utilizing pseudo-peptidic bottlebrush polymers. The influence of a polymer's degree of polymerization on the electro-optic characteristics of PFLC is examined for the first time. Microsphere size, transmittance, contrast ratio, necessary operating voltage, memory effect, and switching speed vary significantly depending on the dopant polymer units in PFLCs. Overall, we proved that a polymer's chain length substantially impacts the performance of PFLC devices.

Chapter 5 investigates the impact of the degree of polymerization on the physical properties of PSLCs. The self-assembly network's structure in PSLCs is controlled by the component polymer, which affects its electrical, dielectric, optical, and electro-optical characteristics. Varying the molecular weight of the doped polymer units results in significant improvements in conductivity, dielectric anisotropy, current, response time, and phase transition temperature. Chapter 6 examines the effect of pseudo-peptidic bottlebrush polymer moieties on the LC director arrangements in droplets. Aromatic and aliphatic appendages are combined with 4-cyano-4'-pentylbiphenyl (5CB) LC, and the phenyl group favors radial formation, while repulsion between 5CB and aliphatic groups drives molecular alignment, resulting in a bipolar droplet arrangement. The study also shows the effect of different pendant groups on the prepared PDLC sample's surface properties and free energy components.

Chapter 7 describes the development of flexible films for thermoelectric generators by doping LCs in carbon nanotubes (CNTs)/polymer composites. This approach simultaneously improves the Seebeck coefficients and electrical conductivity of polyvinylidene fluoride (PVDF) polymer and single-walled carbon nanotubes (SWCNTs)-based composites, resulting in superior thermoelectric potential. LC-based SWCNT/PVDF composites provide a new pathway for creating flexible thermoelectric devices to power wearable electronics. In chapter 8, we briefly discuss the potential uses of LCPCs for flexible devices, beam steering, sensors, drug delivery, tissue engineering, thermoelectric energy harvesting devices and holographic displays. The findings of the thesis provide myriad possibilities for fabricating LCPC-based efficient electro-optic and thermoelectric devices.

सार

लिक्विड क्रिस्टल्स (LCs) कई तकनीकी अनुप्रयोगों में उपयोग किए जा सकते हैं, जिसमें डिस्प्ले उद्योग, दूरसंचार, जीवविज्ञान और ऑप्टिकल टेक्नोलॉजी शामिल हैं। ये आधुनिक उपयोग मौजूदा उद्योग की आवश्यकताओं को पूरा करने के लिए विभिन्न विशिष्ट LC सामग्रियों की मांग करते हैं। उन्नत विशेषताओं वाली नई लिक्विड क्रिस्टल वाली सामग्री का निर्माण करने की कठिनाई के कारण, एलसीपीसी (LCPCs) के संयुक्त रूपों का सुझाव दिया गया है, जो एलसी की विभिन्न गुणवत्ताओं को बढ़ाने के लिए एक विकल्प प्रदान करते हैं, जिसमें मैकेनिकल मजबूती और लचीलापन अधिक होता है। एलसीपीसी का उपयोग गोपनीय खिड़कियों, ऑप्टिकल और इलेक्ट्रो-ऑप्टिकल उपकरण, ऑप्टिकल फिल्टर, स्विचबल टीएचजेडी उपकरण, ऊर्जा हार्वेस्टिंग उपकरण और रासायनिक और बायोसेंसर जैसे विभिन्न उपयोगों में किया जाता है।

पॉलिमर LCs की गुणवत्ता को संशोधित कर सकते हैं, इसे एक निरंतर पॉलिमर मैट्रिक्स बनाकर जिसमें LCs की बूंदें होती हैं, या एक पॉलिमर नेटवर्क के बाईकॉन्टिन्यूस सिस्टम को फैलाकर LCs होस्ट फेज में बिखराया जाता है। इनमें सॉफ्ट मैटर सिस्टम पॉलिमर बिखराया तरल क्रिस्टल (PDLCs), पॉलिमर भरे तरल क्रिस्टल (PFLCs), पॉलिमर स्व-संगठन भरे तरल क्रिस्टल (PSALCs) और पॉलिमर स्थिरित तरल क्रिस्टल (PSLCs) शामिल हैं। हमने पॉलिमरीकरण शर्तों, पॉलिमर मॉर्फोलॉजी और इलेक्ट्रो-ऑप्टिक व्यवहार के बीच इंटरैक्शन को बेहतर समझने के लिए LCPCs के विभिन्न भौतिक गुणों का अध्ययन किया है और इन सिस्टम और सामग्रियों का उपयोग LC आधारित इलेक्ट्रो-ऑप्टिक और ऑप्टिकल उपकरणों के निर्माण के लिए किया गया है। थीसिस के अंत तक, नेमैटिक LC सामग्री का एक संयोजन का उपयोग करके कार्बन नैनोट्यूब (CNTs) और पॉलिविनाइलिडीन फ्लोराइड (PVDF) पॉलिमर मैट्रिक्स के साथ थर्मोइलेक्ट्रिक ऊर्जा हार्वेस्टिंग एप्लिकेशन का अध्ययन किया गया है, और LC आधारित थर्मोइलेक्ट्रिक जनरेटर के विद्युत इलेक्ट्रॉनिक्स और फ्लेक्सिबल डिवाइस के लिए संभावित अनुप्रयोग दर्शाया गया है।

थीसिस के पहले दो अध्याय में LC, पॉलिमर और थर्मोइलेक्ट्रिसिटी के मौलिक अवधारणाओं और गुणों, साथ ही अनुसंधान में उपयोग की गई प्रायोगिक विधियों और तकनीकों का वर्णन किया गया है। अध्याय 3 में, बारियम टाइटेनेट ($BaTiO_3$) नैनोपार्टिकल्स का इपॉक्सी-रेजिन-आधारित PDLC डिवाइस के प्रदर्शन पर प्रभाव प्रस्तुत किया गया है। अध्ययन से पता चलता है कि $BaTiO_3$ नैनोपार्टिकल्स जोड़ने से उपकरण के प्रदर्शन में सुधार होता है, जैसे कि थ्रेशोल्ड वोल्टेज, सैचुरेशन वोल्टेज और राइज टाइम को कम करके कंट्रास्ट अनुपात और यूवी-विसिबल अवशोषण विस्तृति बढ़ाता है। अध्याय 4 में, बायोमेडिकल इंजीनियरिंग और इलेक्ट्रो-ऑप्टिक एप्लिकेशन में बोतलब्रश पॉलिमर के उपयोग का वर्णन किया गया है। कंपोजिट में पॉलिमर, LC, और सॉल्वेंट की घनत्व को बदलकर, LC-बोतलब्रश पॉलिमर कंपोजिट से सबमाइक्रोन से माइक्रोन आकार के संरचनाएं, जैसे कि पोरस नेटवर्क, कण, गोले, एक्स्प्रेसेड, और वेसिकल, बनाई जाती हैं। इसके अलावा, अनुसंधान प्स्यूडोपेप्टिडिक बोतलब्रश पॉलिमर का उपयोग करके पॉलिमर माइक्रोस्फियर से भरे लिक्विड क्रिस्टल (PFLC) से प्रकाश छिताव के स्विच निर्माण की प्रदर्शित करता है। पहली बार PFLC के इलेक्ट्रो-ऑप्टिक विशेषताओं पर पॉलिमर के अधिकतम चरण के प्रभाव का जांच की गई।

माइक्रोस्फियर आकार, पारदर्शिता, कंट्रास्ट अनुपात, आवश्यक ऑपरेटिंग वोल्टेज, मेमोरी प्रभाव, और स्विचिंग स्पीड PFLCs में डोपेंट पॉलिमर इकाइयों पर निर्भर करते हैं। संपूर्ण रूप से, हमने साबित किया कि पॉलिमर की चेन लंबाई PFLC डिवाइस के प्रदर्शन पर बहुत अधिक प्रभाव डालती है।

अध्याय 5 में, PSLC की भौतिक गुणवत्ताओं पर पॉलिमरीकरण के डिग्री के प्रभाव का अध्ययन किया गया है। PSLC में स्व-संयोजन नेटवर्क की संरचना को घटक पॉलिमर द्वारा नियंत्रित किया जाता है, जो इसकी विद्युतीय, द्विविमलता, ऑप्टिकल और इलेक्ट्रो-ऑप्टिकल विशेषताओं पर प्रभाव डालता है। डोप किए गए पॉलिमर इकाइयों के मॉलेक्यूलर वजन को बदलने से चालकता, द्विविमलता असमानता, प्रतिक्रिया समय और फेज परिवर्तन तापमान में काफी सुधार होता है। अध्याय 6 में, प्सेडोपेटिटिक बोटलब्रश पॉलिमर अंशों के प्रतिकूल उच्चकोण फैलाव के लिए LC निर्देशक व्यवस्थाओं पर परीक्षण किया गया है। एरोमेटिक और अलिफैटिक एपेंडेजिस को 4-सायनो-4'-पेंटिलबिफेनाइल (5CB) LC के साथ मिश्रित किया गया है, और फेनाइल समूह रेडियल गठन को पसंद करता है, जबकि 5CB और अलिफैटिक समूहों के बीच का विरोध आकारण निर्देशिका को ड्राइव करता है, जिससे एक द्विध्रुवीय ड्रॉपलेट व्यवस्था होती है। अध्ययन यह भी दिखाता है कि तैयार किए गए PDLC नमूने के सतह गुणों और मुक्त ऊर्जा घटकों पर विभिन्न पेंटेंट समूहों के प्रभाव को कैसे प्रभावित किया जाता है।

अध्याय 7 में, कार्बन नैनोट्यूब (CNT)/पॉलिमर सम्मिश्रण में LC को डोप कर थर्मोइलेक्ट्रिक जेनरेटर के लिए लचीली फिल्मों के विकास का वर्णन किया गया है। इस दृष्टिकोण से, पोलिविनीलीडेंस फ्लोराइड (PVDF) पॉलिमर और एकल-दीवार वाले कार्बन नैनोट्यूब (SWCNT) आधारित सम्मिश्रण के दोनों लचीलापन तथा विद्युत चालकता को सुधारता है, जिससे उत्कृष्ट थर्मोइलेक्ट्रिक क्षमता होती है। LC आधारित SWCNT/PVDF सम्मिश्रण विभिन्न एप्लिकेशन के लिए लचीले इलेक्ट्रो-ऑप्टिक उपकरणों, ऑप्टिकल सेंसर और थर्मोइलेक्ट्रिक ऊर्जा उत्पादन उपकरणों के लिए लचीले विकल्प प्रदान करता है। अध्याय 8 में, हम LCPCs के लचीले उपकरणों, बीम स्टीयरिंग, सेंसर, दवा वितरण, ऊतक अभिविकास, थर्मोइलेक्ट्रिक ऊर्जा अर्जन उपकरण और होलोग्राफिक डिस्प्ले के लिए उनके संभावित उपयोगों पर थोड़ी चर्चा करते हैं। थीसिस के खोज नतीजे LCPC आधारित कुशल वैद्युत वैद्युतिक और थर्मोइलेक्ट्रिक उपकरणों को बनाने के लिए असीमित संभावनाओं को खोलते हैं।

TABLE OF CONTENTS

CERTIFICATE	i
ACKNOWLEDGEMENTS	ii
ABSTRACT	iv
TABLE OF CONTENTS	viii
LIST OF FIGURES	xiii
LIST OF TABLES	xxii
LIST OF ABBREVIATIONS	xxiii
LIST OF SYMBOLS	xxiv
CHAPTER 1: INTRODUCTION	1
1.1. Background	1
1.2. Classification of LCs	2
1.3. Physical Properties of LCs	3
1.3.1. Anisotropy	4
<i>1.3.1.1. Dielectric Anisotropy</i>	4
<i>1.3.1.2. Birefringence</i>	4
1.3.2. Elastic constants	5
1.3.3. Threshold voltage	6
1.3.4. Order parameter	6
1.4. Polymers	7
1.5. Liquid Crystal-polymer composites (LCPCs)	8
1.5.1. Broad classification of LCPCs	9
<i>1.5.1.1. Polymer Dispersed Liquid Crystals (PDLCs)</i>	9
<i>1.5.1.2. Polymer-filled liquid Crystals (PFLCs)</i>	12
<i>1.5.1.3. Polymer Stabilized Liquid Crystals (PSLCs)</i>	12
<i>1.5.1.4. Polymer Self-Assembly Filled with Liquid Crystal (PSALC)</i>	13
1.5.2. Characteristics features of LCPCs	13
<i>1.5.2.1. Dynamic Light Scattering</i>	13
<i>1.5.2.2. Off-state transmittance (T_{off})</i>	16
<i>1.5.2.3. On-state transmittance (T_{on})</i>	16
<i>1.5.2.4. Contrast Ratio</i>	16
<i>1.5.2.5. Switching Voltages</i>	16
<i>1.5.2.6. Response time</i>	17
<i>1.5.2.7. Hysteresis effect</i>	17

1.6. Thermoelectricity	17
1.6.1. Thermoelectric (TE) Effect	18
1.7. Motivation	19
1.8. Objectives	20
1.9. Outline of Thesis	21
1.10. Conclusion	24
References	24
CHAPTER 2: EXPERIMENTAL TECHNIQUES	30
2.1 Fabrication of cells	30
2.2. Characterization techniques:	32
2.2.1 Thermal Characterizations	32
2.2.1.1. <i>Thermogravimetric analysis</i>	32
2.2.1.2. <i>Differential scanning calorimetry (DSC)</i>	33
2.2.2 Morphological Characterizations	34
2.2.2.1. <i>Polarized optical microscopy</i>	34
2.2.2.2. <i>Atomic Force Microscopy</i>	36
2.2.2.3. <i>Scanning Electron Microscopy</i>	37
2.2.2.4. <i>Field Emission Scanning Electron Microscopy (FESEM)</i>	39
2.2.3. Structural Characterizations	39
2.2.3.1. <i>Raman Spectroscopy</i>	40
2.2.3.2. <i>Fourier-Transform Infrared (FTIR) Spectroscopy</i>	41
2.2.4. Optical Characterizations	42
2.2.4.1. <i>UV-visible Spectroscopy</i>	42
2.2.4.2. <i>Contact Angle Measurement</i>	43
2.2.5. Electro-optic Characterization	44
2.2.6. Electrical Characterizations	45
2.2.6.1. <i>Dielectric spectroscopy</i>	45
2.2.6.2. <i>Thermoelectric measurements</i>	48
2.3. Analysis of error and experimental precision	50
2.4. Conclusion	52
References	52
CHAPTER 3: DESIGN AND FABRICATION OF EPOXY-RESIN-BASED PDLCS AND ROLE OF BATIO₃ NANOPARTICLES ON THE ELECTRO-OPTIC PERFORMANCE OF PDLC DEVICES	55
3.1. Introduction	55

3.2. Experimental details	56
3.3. Result and discussion	58
3.3.1. Texture and morphology	58
3.3.2. Electro-optic properties	60
3.3.3. Rise & fall time	65
3.3.4. UV-visible spectroscopy	66
3.4. Conclusion	68
References	69

CHAPTER 4: PSEUDOPEPTIDIC BOTTLEBRUSH BASED ENCAPSULATION OF LC IN POLYMER VESICLES AND PSEUDOPEPTIDIC POLYMER MICROSPHERE-FILLED LC **72**

4.1. Introduction	72
4.1.1. Bottlebrush Polymer-Liquid Crystal composites and vesicles	72
4.2. Experimental details	73
4.2.1. Vesicles preparation and characterization details	73
4.3. Result and discussion	75
4.3.1. Composites and Vesicles	75
4.3.1.1. <i>Morphology of Composites</i>	75
4.3.1.2. <i>Texture of Vesicles</i>	75
4.3.1.3. <i>Vesicles size and Raman mapping</i>	76
4.3.1.4. <i>Contact angle measurement and surface characteristics</i>	77
4.1.2. Bottlebrush polymer microsphere-filled liquid crystal switches	79
4.2.2. Light scattering switches fabrication and characterization details	80
4.3.2. Characterization of light scattering switches	81
4.3.2.1. <i>Morphology</i>	82
4.3.2.2. <i>Fourier-Transform Infrared Spectroscopy (FTIR)</i>	84
4.3.2.3. <i>Textural and Thermal Characterization</i>	85
4.3.2.4. <i>Electro-optic Characterization</i>	87
4.3.2.5. <i>Response time measurement</i>	91
4.3.2.6. <i>Optical characterization</i>	92
4.4. Conclusion	94
References	95

CHAPTER 5: PSEUDOPEPTIDIC BOTTLEBRUSH POLYMERS FOR MODULATING ELECTRO-OPTIC SWITCHING, DIELECTRIC AND ELECTRICAL PROPERTIES OF LC **98**

5.1. Introduction	98
5.2. Experimental details	99
5.3. Results and discussion	101
5.3.1. Texture and morphology	101
5.3.2. Dielectric and electrical characterization	104
5.3.3. Electro-optic properties	110
5.3.4. Response time	112
5.3.5. Optical characterization	113
5.4. Conclusion	114
References	115

CHAPTER 6: CONTROL ON LC DIRECTOR CONFIGURATION USING PSEUDOPEPTIDIC BOTTLEBRUSH POLYMERS **118**

6.1. Introduction	118
6.2. Experimental details	120
6.3. Result and discussion	123
6.3.1. Thermal stability and optical microscopy	123
6.3.2. FESEM characterization	127
6.3.3. Contact angle measurement	129
6.3.4. pH effect analysis	131
6.4. Conclusion	134
References	134

CHAPTER 7: SYNERGETIC ENHANCEMENT OF SEEBECK COEFFICIENT AND ELECTRICAL CONDUCTIVITY IN FLEXIBLE LC COMPOSITES **138**

7.1. Introduction	138
7.2. Experimental details	141
7.3. Result and discussion	142
7.3.1. Thermoelectric Characterization	142
7.3.2. Hall Measurement	148
7.3.3. Raman Characterization	150
7.3.4. Morphology of Composites	151
7.3.5. Tensile Strain Measurement	154
7.3.6. Thermoelectric Performance	154
7.4. Conclusion	158
References	159

CHAPTER 8: CONCLUSION AND FUTURE SCOPE	162
8.1. Conclusion	162
8.2. Future Scope	164
AUTHOR'S BIOGRAPHY	167
LIST OF PUBLICATIONS	168

LIST OF FIGURES

Fig. 1.1: A schematic illustration of the LC phase on the temperature scale.	1
Fig. 1.2: Diagram illustrating the categorization of LCs.	2
Fig. 1.3: Schematic representation of calamitic LC.....	3
Fig. 1.4: (a) Calamitic LCs general template and (b) chemical structure of 5CB.	3
Fig. 1.5: Schematic of LC director configurations (a) splay, (b) twist, and (c) bend.	5
Fig. 1.6: Schematic illustration of the LC order parameter; \hat{n} denotes the LC director, and θ represents the angle between the director and the LC molecules' long axis.....	6
Fig. 1.7: Schematics of a PDLC sample in the <i>off</i> -state in the absence of, and <i>on</i> -state in the presence of, an electric field	10
Fig. 1.8: Schematic of (a) radial and (b) bipolar LC director arrangement in droplets.	11
Fig. 1.9: Schematic of PFLC sample in an <i>off</i> -state in the absence and <i>on</i> -state in the presence of the electric field.	12
Fig. 1.10: Schematic of PSLC in an <i>off</i> -state in the absence and <i>on</i> -state in the presence of the electric field.	13
Fig. 1.11: Illustration of scattering by single droplet model at an applied voltage (a) $V = 0$, (b) $V < V_{th}$, (c) $V \geq V_{th}$, and (d) $V \geq V_{sat}$	14
Fig. 1.12: A schematic of the Seebeck effect.....	18
Fig. 2.1: Schematic illustration of LC director orientation in (a) homogeneous and (b) homeotropic LC cell.	30
Fig. 2.2: Steps to fabricate an unaligned LC cell.....	31
Fig. 2.3: (a) Schematic and (b) photograph of the thermogravimetric analysis (TGA) setup.	33
Fig. 2.4: Differential scanning calorimetry (DSC) (a) Schematic and (b) photograph of TA instruments DSC 2500.	34

Fig. 2.5: (a) Photograph of OLYMPUS BX-51P POM and (b) schematic illustration (polarizer and Analyzer are crossed).....	35
Fig. 2.6: Uniformly aligned uniaxial LC to define different angles used to describe transmitted intensity.....	36
Fig. 2.7: (a) Schematic of AFM system indicating various components and operating in different modes [16], and (b) experimental setup of AFM system (Bruker Dimension Icon scanning probe microscope).	37
Fig. 2.8: (a) Schematic diagram of the scanning electron microscope (SEM), (b) magnified view of interaction volume, and (c) Camera picture of JEISS EVO50 SEM.....	38
Fig. 2.9: Photograph of FESEM instrument of model name JEOL JSM-7800F Prime.	39
Fig. 2.10: An energy level diagram depicting the various energy transitions is shown in Raman Spectroscopy.....	40
Fig. 2.11:LABRAM HR Raman spectrometer photograph.	41
Fig. 2.12: Schematic diagram of FTIR spectroscopy.	42
Fig. 2.13: (a) The PerkinElmer UV-vis spectrophotometer, NRF IIT Delhi, and (b) the reflectance and transmittance measurements are shown schematically.	43
Fig. 2.14: Schematic representation of UV-vis spectrometer.....	43
Fig. 2.15: Schematic for contact angle measurement setup.....	44
Fig. 2.16: Schematic of the electro-optic experimental setup.....	45
Fig. 2.17: Image of the experimental setup for dielectric measurements during a live experiment.....	47
Fig. 2.18: Linseis LSR-3 system employed to measure the Seebeck coefficient and electrical resistivity.....	50
Fig. 3.1: TEM images in which darker areas indicate BaTiO ₃ nanoparticles.....	57

Fig. 3.2: The morphological behaviour of (a) undoped PDLC (b) 0.25 wt% (c) 0.33 wt% (d) 0.4 wt% (e) 0.47 wt% (f) 0.55 wt% BaTiO ₃ doped PDLC samples as observed under crossed polarizer and analyzer.	58
Fig. 3.3: SEM images of (a) undoped, (c) 0.47 wt%, and (d) 0.55 wt% doped are captured at 5.00 k, and (b) 0.33 wt% doped is captured at 10.00 k. The circled regions show the aggregation of nanoparticles in 0.47 and 0.55 wt%.....	59
Fig. 3.4: Transmission curve at room temperature.	61
Fig. 3.5: Photograph of fabricated 0.55 wt% BaTiO ₃ doped sample (a) in the absence of field and (b) in the presence of 20 V _{pp} applied voltage.	61
Fig. 3.6: (a) Variation of required threshold and saturation voltages and (b) CR ratio and <i>off</i> -state transmission for the PDLC film as a function of BaTiO ₃ doping concentration.	62
Fig. 3.7: Capacitance of pure and nanoparticle doped PDLC films.	63
Fig. 3.8: Hysteresis obtained in electro-optic response of (a) pure and (b) 0.5 wt% doped sample. Top and bottom inset are the POM images at 0, and 15 V _{pp} applied voltage, respectively.	64
Fig. 3.9: (a) Response time, (b) Rise, and (c) fall intensity response for the undoped and BaTiO ₃ doped samples.	65
Fig. 3.10: (a) The <i>off</i> -state transmission and (b) absorption curve obtained by UV- visible spectroscopy. Calculated (c) absorption and (d) scattering coefficient <i>vs.</i> wavelength for undoped and doped samples.	67
Fig. 3.11: Haze value with wavelength variation.	68
Fig. 4.1: Chemical structure of bottlebrush polymer PF.....	74
Fig. 4.2: FESEM images of (a) porous network, (b) aggregates, (c) microspheres, (d) particles, and (e) vesicles.....	75
Fig. 4.3: (a-b) OM images of PF and PF ₃ sample. (c-f) POM images of PF, PF ₁ , PF ₂ , and PF ₃ , respectively.	76

Fig. 4.4: (a, c) FESEM images and (b, d) vesicle size distribution of PF and PF ₃ samples, respectively.	76
Fig. 4.5: 2D AFM image of (a) PF, (b) PF ₂ , and (c) PF ₃ , (d) Raman band corresponding to C≡N stretching vibration at 2227 cm ⁻¹ . Raman mapping images for vesicles of (e) PF ₂ and (f) PF ₃	77
Fig. 4.6: Contact angle of (a-d) distilled water and (e-h) diiodomethane on PF, PF ₁ , PF ₂ , and PF ₃ films, respectively. (i) surface energy, dispersive and (j) polar part obtained using contact angle measurement, (k) UV-vis spectrum of composites solution.	78
Fig. 4.7: Optical microscopic images (pseudo-colors are used to create images) of PFLC samples after the removal of LC molecules a) PFL-5CB, b) PFM-5CB, and c) PFH-5CB. Captured at 100× magnification, Bar scale- 10 μm.	82
Fig. 4.8: (a-c) FESEM images, (d-f) 3D AFM images of PFLC samples PFL-5CB, PFM-5CB, and PFH-5CB, respectively.	82
Fig. 4.9: POM texture of (a) PFL-5CB, (b) PFM-5CB, and (c) PFH-5CB, bottom inset is the microsphere size distribution measured through POM. Microsphere size distribution obtained via FESEM of (d) PFL-5CB, (e) PFM-5CB, and (f) PFH-5CB, respectively.	83
Fig. 4.10: FESEM image of (a) PFH-7CB film after removing excess LC molecules and (b) pure PFH film	84
Fig. 4.11: FESEM images of (a) 1PFH and (b) 4PFH PFLC samples.	84
Fig. 4.12: FTIR spectra of pure 5CB, pure PFH, and PFH-5CB sample after the removal of LC.	85
Fig. 4.13: POM image of PFLC sample (a) PFL-5CB, (b) PFM-5CB and (c) PFH-5CB, images are captured at 25°C. The top and bottom insets are the images captured during the heating and cooling cycle, respectively.	85
Fig. 4.14: DSC curve of (a) PFM and (b) PFLC composites.	86
Fig. 4.15: (a) Transmittance vs. voltage curve (b) required operating voltages, (c) off- and on-state transmittance value, and (d) CR ratio of PFLC samples.	87

Fig. 4.16: Transmittance vs. voltage curve of PFLC composites with horizontal (H) and vertical (V) polarized laser beam.....	90
Fig. 4.17: Transmittance vs. voltage curve of concentration variants PFLC composites of (a) PFL, (b) PFM, and (c) PFH and (d) LC:polymer/80:20 wt% composites of PFL, PFM, and PFH polymer in a 6-micron cell.....	90
Fig. 4.18: (a) Prototype of prepared PFLC samples, (b) <i>off</i> -state and (c) <i>on</i> -state of fabricated PFM-5CB sample after applying 40 V_{pp}	91
Fig. 4.19: (a) rise and fall time and (b) intensity variation with application and removal of the electric field of PFLC composites.....	92
Fig. 4.20: (a) <i>off</i> -state transmission and (b) haze variation with wavelength for different PFLC samples.....	93
Fig. 5.1: The polymer network and the orientation of the LC molecules in a PSLC cell are shown schematically, both in the absence of an applied voltage and in the presence of an applied voltage.....	100
Fig. 5.2: Schematic representation of the electro-optic setup.....	101
Fig. 5.3: (a) Chemical structure of bottlebrush polymer PF. POM images of (b, f) 5CB, (c, g) PFL-SLC, (d, h) PFM-SLC, and (e, i) PFH-SLC at room temperature by keeping circular stage at 0° and 45°, respectively.....	102
Fig. 5.4: POM images under crossed polarizer of PFL-SLC samples with (a) 2 wt% and (b) 4 wt% PFL showing the size of polymer aggregates increases with the concentration of the dopant polymer. The scale bar indicates 100 μm	102
Fig. 5.5: The microscopic images of PFL-SLC, PFM-SLC, and PFH-SLC samples, respectively, (a-c) FESEM and (d-f) AFM; Inset shows the magnified images.....	103
Fig. 5.6: LC domain size distribution as obtained from POM images of (a) PFL-SLC, (b) PFM-SLC, and (c) PFH-SLC sample.....	103
Fig. 5.7: POM images under crossed polarizer of (a) 5CB, (b) PFM-SLC, (c) PFH-SLC during the heating cycle.....	104

Fig. 5.8: Variation of (a-b) dielectric constant (ϵ') and (c-d) dielectric loss (ϵ'') vs. log f for 5CB and PFL-SLC sample at different temperatures; (e) dielectric constant and (f) dielectric loss for 5CB and PSLC samples at 30°C temperature.....	106
Fig. 5.9: (a) Dielectric constant, (b) dielectric loss of 5CB and PFL doped samples.....	107
Fig. 5.10: Uemura fitted low frequency peak of dielectric loss at 40°C temperatures (a) 5CB and (b) PFH-SLC.....	107
Fig. 5.11: Variation of mobile ion concentration (a) n_1 , (b) n_2 , and diffusion coefficient (c) D_1 and (d) D_2 with temperature in 5CB and PSLC samples.....	108
Fig. 5.12: (a) Changes in capacitance with voltage variation. (Inset shows the dielectric anisotropy ($\Delta\epsilon$) for 5CB and PSLC samples at 25°C temperature), (b) Conductivity curve as a function of frequency at different temperatures, and (c) I - V curve for 5CB and PSLC samples.....	110
Fig. 5.13: (a) Transmittance vs. voltage (T - V) curve. (Inset shows the value of threshold voltage) and (b) Change in optical transmittance with rotation of a polarizer angle.....	111
Fig. 5.14: (a) Transmittance vs. voltage (T - V) curve, and (b) optical transmittance with rotation of a polarizer angle.....	111
Fig. 5.15: (a) Rise, fall, and response time of 5CB and PSLC samples, and (b) response time of 5CB and PFL doped samples.....	112
Fig. 5.16: UV-vis absorption spectra of 5CB and prepared PSLC samples. (Inset shows the band gap values)	114
Fig. 6.1: Schematic diagram and POM images of LC director configuration in the droplets (a, c) radial and (b, d) bipolar, respectively.	119
Fig. 6.2: Chemical structures of pseudopeptidic bottlebrush polymers PFO, PFH, PEO, and PEH based on Phe and Glu-amino acids.....	121
Fig. 6.3: POM image of PDLC sample prepared using 50 wt% PEO polymer and 50 wt% 5CB having solution concentration (a) 5% w/v, and (b) 10% w/v.	122
Fig. 6.4: Thermogravimetric analysis (TGA) profile of PFO, PFH, PEO, and PEH.....	124

Fig. 6.5: Optical microscope (OM) images of (a) PFO and (b) PEO films. POM images of (c) 5CB (inset shows bipolar droplets during isotropic to nematic transition), (d) PFO6, (e) PFO5, (f) PFO4, (g) PFH5, (h) PEO6, (i) PEO5, (j) PEO4, (k) PEH5 and (l) PEH4 sample..... 125

Fig. 6.6: POM image of pure PFO polymer film..... 125

Fig. 6.7: Droplet size obtained using POM images of (a) PFO6, (b) PFO5, (c) PFO4, (d) PFH5, (e) PEO6, (f) PEO5, (g) PEO4, (h) PEH5 and (i) PEH4 samples..... 126

Fig. 6.8: (a, c) POM and (b, d) OM images of radial and bipolar droplets in PFO5 and PEO5 samples, respectively. (e - h) radial, and (i - l) bipolar LC droplet by rotating the crossed polarizer position w.r.t. samples at an angle of 0°, 45°, 65°, and 90°, respectively. The red dotted line shows the rotation of the Maltese brushes and defect lines. 127

Fig. 6.9: FESEM images of (a) PFO, (b) PFO6, (c) PFO5, (d) PFO4, (e) PEO, (f) PEO6, (g) PEO5, and (h) PEO4 sample. The droplet distribution obtained through FESEM images is shown in the inset images. 128

Fig. 6.10: FESEM images of (a) PFH, (b) PFH5, (c) PEH, and (d) PEH5 sample. 128

Fig. 6.11: The minor to major axis (b/a) ratio of the droplets calculated using FESEM images of (A) PFO and (B) PEO samples..... 129

Fig. 6.12: (a) Contact angle with diiodomethane, formamide, and water (red dotted lines indicate the window of the moderate hydrophilic region), and (b, c) total surface free energy and its components of pure polymer and prepared PDLC samples at 50 wt% of each polymer and LC..... 129

Fig. 6.13: Contact angle of PFO6, PFO4, PFH4, PEO6, PEO4, and PEH4 PDLC sample with diiodomethane, formamide, and water..... 130

Fig. 6.14: Total surface free energy and its components of PFO6, PFO4, PFH4, PEO6, PEO4, and PEH4 PDLC sample..... 131

Fig. 6.15: POM images under crossed polarizers of PFO5 and PEO5, respectively (A, B) in the absence of pH and after drop-casting the solution of pH (a) 4, (b) 6.8, (c) 7, (d) 8.8, and (e) 10. 132

Fig. 6.16: POM images under crossed polarizers of PFO5 and PEO5 sample after the drop-casting solution of pH (a, d) 4, (b, e) 7, and (c, f) 10.....	133
Fig. 7.1: Experimental steps involved in preparing a free-standing composite sample.	142
Fig. 7.2: (a, d) Seebeck coefficient, (b, e) electrical conductivity, and (c, f) power factor of the prepared LC composite films using S1, and S2 samples, respectively.....	143
Fig. 7.3: (a) Seebeck coefficient, (b) electrical conductivity, and (c) power factor of the prepared composite films using PVDF/MWCNT with and without LC.	144
Fig. 7.4: (a) Seebeck coefficient, (b) electrical conductivity, and (c) power factor of the prepared composite films using cellulose acetate (CA)/MWCNT with and without LC.....	145
Fig. 7.5: Band diagrams (a) before and (b) after alignment, illustrating the energy-filtering impact at the interfaces among LC (5CB) and SWCNTs.....	146
Fig. 7.6: (a) Carrier concentrations (n), and (b) carrier mobility (μ) of SWCNTs composites based flexible films.....	149
Fig. 7.7: Raman spectra of (a) pure SWCNTs and composite films made of SWCNTs composites and (b) expanded spectra of the RBM peak from 100 to 300 cm^{-1}	151
Fig. 7.8: Raman spectra of pure MWCNTs and composite films made of (a) PVDF and (b) CA.	151
Fig. 7.9: FESEM images of (a) S1, (b) S1-5CB10, (c) S1-5CB50, (d) S2, (e) S2-5CB10, and (f) S2-5CB50 composite flexible films.....	152
Fig. 7.10: (a, b) and (c, d) is the FESEM image of 10 wt % and 15 wt% MWCNT composite films using PVDF and cellulose acetate, respectively.....	152
Fig. 7.11: Average pore diameter obtained using FESEM images of (a) S1-5CB50 and (b) S2-5CB50 composite flexible films.	153
Fig. 7.12: POM and FESEM image of (a, c) pure PVDF and (b, d) PVDF(50 wt%)/LC(50wt%) composite film; the inset shows the LC domain size.....	153
Fig. 7.13: Stress vs. strain curve of SWCNT/PVDF composites.....	154

Fig. 7.14: (a) TEG device schematic, and (b) output voltage curve in open circuit with temperature gradient variations.....155

Fig. 7.15: Curve of output voltage dependence of the temperature difference..... 155

Fig. 7.16: Voltage *vs.* current (*V-I*) curve of TEG prepared using (a) SWCNT/PVDF and (b) MWCNT/PVDF composite film..... 156

Fig. 7.17: Current *vs.* output voltage and current *vs.* output power of the S1-5CB10 TEG device at a temperature difference of 60 K. 157

LIST OF TABLES

Table 4.1: Composition of prepared vesicle samples.	74
Table 4.2: Molecular weight distribution of polymers.	81
Table 4.3: PFLC samples prepared by using different wt % of LC and polymer.....	81
Table 4.4: PTT values during heating and cooling of PFLC samples.	85
Table 5.1: Molecular weight distribution of polymers as obtained from GPC.....	100
Table 5.2: PTT temperature for 5CB and PSLC samples.....	104
Table 5.3: Dielectric anisotropy values for 5CB and PSLC samples.	113
Table 6.1: Composition of different PDLC samples used in this study.....	122
Table 6.2: Molecular weight distribution of polymers obtained from GPC using THF as eluent.	123
Table 6.3: Phase transition temperature of the prepared PDLC samples.	127
Table 7.1: Different SWCNT-based flexible composite films are prepared by varying the wt% of the used components.....	141
Table 7.2: Different MWCNT-based flexible composite films prepared by varying the wt% of the used components.....	141
Table 7.3: Comparison of thermoelectric performance of PVDF/SWCNT composites with literature.....	158

LIST OF ABBREVIATIONS

LC: Liquid crystal	HRTEM: High resolution and transmission electron microscopy
LCD: Liquid crystal display	CRT: Cathode ray tube
LCPCs: Liquid crystal polymer composites	EDX: Energy dispersive x-ray spectroscopy
PDLCs: Polymer-dispersed liquid crystals	FTIR: Fourier transform infrared spectroscopy
PFLCs: Polymer-filled liquid crystals	UV-vis: UV-visible
PSLCs: Polymer-stabilized liquid crystals	CA: Contact angle measurement
PSALCs: Polymer self-assembly filled with liquid crystals	NIR: Near infrared
TIPS: Thermally induced phase separation	IR: Infrared
PIPS: Polymerization-induced phase separation	E-O: Electro-optic
SIPS: Solvent-induced phase separation	BaTiO ₃ : Barium titanate
TE: Thermoelectric	5CB: 4-Cyano-4'-pentylbiphenyl
TEG: Thermoelectric generator	7CB: <i>4'-Heptyl-4-biphenylcarbonitrile</i>
UV: Ultra-violet	PPGDE: Polypropylene glycol diglycidyl ether
ITO: Indium tin oxide	EGDE: Ethylene glycol diglycidyl ether
IPA: Isopropyl alcohol	DETA: Diethylenetriamine
DI: Deionized	CR: Contrast ratio
TGA: Thermogravimetric analysis	PF: Peptide-based bottlebrush homopolymer
DSC: Differential scanning calorimetry	PTT: Phase transition temperature
OM: Optical microscopy	WCA: Water-to-air contact angle
POM: Polarizing optical microscopy	SFE: Surface free energy
AFM: Atomic force microscopy	SWCNT: Single-wall carbon nanotubes
SEM: Scanning electron microscopy	MWCNT: Multi-wall carbon nanotube
FESEM: Field emission scanning electron microscopy	

LIST OF SYMBOLS

$\Delta\epsilon$: Dielectric Anisotropy	T : Temperature
n_e : Extraordinary refractive index	E_g : Band gap
n_o : Ordinary refractive index	λ : Wavelength
Δn : Birefringence	V_{th} : Threshold voltage
\hat{n} : Liquid crystal director	V_{sat} : Saturation voltage
<i>o-ray</i> : Ordinary ray	I_i : Incident light intensity
<i>e-ray</i> : Extraordinary ray	I_t : Transmitted light intensity
K_{11} : Splay elastic constant	T_{off} : Off state transmission
K_{22} : Twist elastic constant	T_{on} : On state transmission
K_{33} : Bend elastic constant	τ_{on} : Rise time
V_{pp} : Peak to peak voltage	τ_{off} : Fall time
ϵ_o : Free space permittivity	τ : Response time
ϵ^* : Complex dielectric permittivity	S : Seebeck coefficient
ϵ' : Real part of dielectric permittivity	σ : Electrical conductivity
ϵ'' : Imaginary part of dielectric permittivity	N : Carrier concentration
$\tan \delta$: Dielectric loss factor	μ : Mobility
D : Diffusion coefficient	κ : Thermal conductivity
k_B : Boltzmann constant	ZT : figure of merit